

Preparation of Fe-rich giant magnetocaloric (Mn,Fe) $_2$ (P,Si) ribbons and calorimetric analysis of the first-order magnetic transition

Hanggai, W.; Yibole, H.; Guillou, F.; Kwakernaak, C.; van Dijk, N. H.; Brück, E.

DOI

10.1016/j.actamat.2025.121677

Publication date

Document Version Final published version Published in Acta Materialia

Citation (APA)
Hanggai, W., Yibole, H., Guillou, F., Kwakernaak, C., van Dijk, N. H., & Brück, E. (2026). Preparation of Ferich giant magnetocaloric (Mn,Fe) (P,Si) ribbons and calorimetric analysis of the first-order magnetic transition. *Acta Materialia*, *302*, Article 121677. https://doi.org/10.1016/j.actamat.2025.121677

Important note

To cite this publication, please use the final published version (if applicable). Please check the document version above.

Copyright

Other than for strictly personal use, it is not permitted to download, forward or distribute the text or part of it, without the consent of the author(s) and/or copyright holder(s), unless the work is under an open content license such as Creative Commons.

Please contact us and provide details if you believe this document breaches copyrights. We will remove access to the work immediately and investigate your claim.

ELSEVIER

Contents lists available at ScienceDirect

Acta Materialia

journal homepage: www.elsevier.com/locate/actamat





Preparation of Fe-rich giant magnetocaloric (Mn,Fe)₂(P,Si) ribbons and calorimetric analysis of the first-order magnetic transition

W. Hanggai ^{a,*} , H. Yibole ^b , F. Guillou ^{b,c}, C. Kwakernaak ^d , N.H. van Dijk ^a , E. Brück ^a

- ^a Fundamental Aspects of Materials and Energy (FAME), Faculty of Applied Sciences, Delft University of Technology, Mekelweg 15, 2629JB Delft, The, Netherlands ^b College of Physics and Electronic Information, Inner Mongolia Key Laboratory, for Physics and Chemistry of Functional Materials, Inner Mongolia Normal University,
- ^c Normandie University, ENSICAEN, UNICAEN, CNRS, CRISMAT, Caen 14000, France
- d Department of Materials Science and Engineering, Delft University of Technology, Mekelweg 2, 2628 CD Delft, The Netherlands

ARTICLE INFO

81 Zhaowuda Rd., Hohhot 010022, China

Keywords: Magnetocaloric effect Magneto-elastic coupling Phase transition Heat capacity Elastic strain energy Latent heat

ABSTRACT

The $(Mn,Fe)_2(P,Si)$ compounds are one of the rare materials systems that exhibit an isostructural first-order ferromagnetic transition (FOMT) near ambient temperature. Since the discovery of its giant magnetocaloric effect (GMCE), this system is garnering ongoing interest, both for its promising performances for applications and for the scientific interest in uncovering the fundamental mechanisms driving the FOMT. This study examines the evolution of the structure, the microstructure, the thermal and magnetic properties in $Mn_{0.60+x}Fe_{1.3-x}P_{0.66-y}Si_{0.34+y}$ ($0 \le x \le 0.08, x = 2y$) compounds prepared by the melt-spun technique. The simultaneous increase in Mn and Si concentrations leads to a 40 % enhancement in the isothermal entropy change ($|\Delta S_{max}|$) compared to parent compound. Furthermore, we propose a method to separate the latent heat (L) from the reversible specific heat. This allows us to establish a convincing correlation between two intrinsic quantities, the latent heat (L) and the elastic strain energy (U_e). Our results demonstrate that both latent heat (L) and thermal hysteresis (ΔT_{hvs}) are proportionally linked and vanish simultaneously at a critical end point.

1. Introduction

The magnetocaloric effect (MCE) is an intrinsic magneto-thermal phenomenon that links a sudden change in the magnetic field to a temperature change in a material, thereby enabling magnetic refrigeration technologies [1–10]. The MCE is characterized by the isothermal entropy change (ΔS) or the adiabatic temperature change ($\Delta T_{\rm ad}$), depending on whether the magnetic field change is applied isothermally or adiabatically. When the MCE for different materials is compared, it is important to note that a large $|\Delta S|$ does not always correspond to a large $\Delta T_{\rm ad}$, so both quantities must be optimized simultaneously [5,11]. Integrating this effect opens up novel possibilities for magnetic cooling [2,4,12,13], heat pumping [14–18], and energy conversion, such as thermomagnetic harvesting applications [19,20]. These applications present a higher energy efficiency and do not use greenhouse gases, and could therefore contribute to mitigate the climate change.

A giant magnetocaloric effect (GMCE) is typically associated with a first-order magnetic transition (FOMT). Depending on their intrinsic mechanisms, the FOMT can be classified into two types: the magneto-

elastic transition that does not change the crystal symmetry, as observed in materials like $La(Fe,Si)_{13}$ [21–23], FeRh [24,25], Eu_2In [26] and $(Mn,Fe)_2(P,Si)$ [4,6], and the magneto-structural transition, where the change in magnetic state is associated with a change in crystal symmetry, as found in compounds such as $Gd_5(Si,Ge)_4$ [27], MnMX TiNiSi-Ni $_2In$ [28,29] and NiMn-based Heusler alloys [30,31], etc. Among these different material systems, the Fe $_2P$ -based compounds, particularly $(Mn,Fe)_2(P,Si)$, stand out as one of the most promising for real application due to their low raw material costs, absence of rare earth elements, the absence of toxic elements and a tuneable Curie temperature near room temperature. These features make this system especially suitable for eco-sustainable applications.

Besides their advantages, the present systems with a GMCE at a FOMT often also have negative aspects such as thermal hysteresis ($\Delta T_{\rm hys}$), which impers the reversibility of the effect [7,32] and mechanical embrittlement. Previous studies on MnFe(P,Si) materials have shown that reducing the hysteresis can be achieved by adjusting the Mn/Fe and P/Si ratios. However, this adjustment typically leads to a decrease in magnetization. To enhance both the magnetization and ΔM ,

E-mail address: H.Gai@tudelft.nl (W. Hanggai).

^{*} Corresponding author.

it is necessary to work near the MnFeP2/3Si1/3 composition, which represents a dual optimum for achieving a high saturation magnetization [33,34]. At the FOMT, not only a sharp magnetization jump is observed, but also discontinuities in other physical parameters are found [35]. For the (Mn,Fe)₂(P,Si) system at the ferromagnetic transition temperature (T_C) , the unit-cell contracts in the hexagonal basal plane across the FOMT, while it expands along the hexagonal axis. This overall lattice deformation results in a discontinuity in c/a ratio reaching up to 10 %, while the unit-cell volume change $\Delta V/V = 0.1$ –0.3 % is nearly negligible. Such discontinuities can induce strong shear strains and stresses at the grain boundaries in random orientated polycrystals, particularly for larger grains. Thermal or magnetic field cycling potentially results in the formation of fractures or even the destruction of the bulk materials. These issues can be addressed by technical solutions, such as embedding the MCE material in a resin or using porous shaping techniques. However, these approaches will dilute the MCE effect, which is unwanted as it results in an inefficient use of the magnetic field source. In recent years, numerous studies have explored the introduction of a fifth element. This includes doping with 3d through 5d transition metals [32,36-40], which can potentially fine-tune the Curie temperature ($T_{\rm C}$) and reduce $\Delta T_{\rm hys}$. Substitutions of P by As, Ge, Al and B have also been investigated as potential dopants [41–45]. However, from the perspectives of layering the transition temperatures along the regenerator or for scaling-up the synthesis, multiplying the number of elements with small quantities of substitutions raises some challenges.

Here, we tackle the above issue by compositional control and manipulating the microstructure to achieve smaller grain sizes. On the Fe-rich side of the (Mn,Fe)₂(P,Si) phase diagram, higher Si concentrations result in smaller discontinuities in Δa and Δc across the FOMT [6, 46]. At the same time, metallurgical challenges have been widely reported in the Mn-Fe-P-Si system. Previous studies have predominantly employed ball-milling methods [32,34,36,45]. Samples prepared by this conventional approach often display significant porosity [64,66], which adversely affects thermal conductivity. Furthermore, this family of materials is highly sensitive to the purity of the starting elements, often leading to the formation of secondary phases such as (Mn,Fe)₃Si [66]. In contrast, melt spinning, which combines liquid-phase segregation with rapid solidification, enables the synthesis of fine-grained, single-phase materials [46]. The refinement of grains can mitigate shear strains and stresses at grain boundaries, thereby enhancing mechanical stability, which is particularly critical given the intrinsic brittleness of these compounds. Despite these advances, a systematic comparison of the microstructural features between conventionally processed and melt-spun samples remains unexplored. Therefore, in this work, we employ the melt-spinning technique to investigate both the microstructure and magnetic properties of Mn_{0.60+x}Fe_{1.3-x}P_{0.66-y}Si_{0.34+y}

The $Mn_{0.60+x}Fe_{1.3-x}P_{0.66-y}Si_{0.34+y}$ compounds presently studied show a strengthening of the FOMT characteristics (hysteresis, discontinuity, specific heat peak), which led us to investigate the evolution of the latent heat (L) along this series. While the latent heat is an intrinsic quantity highly relevant for the development of GMCMs, its separation from the reversible specific heat background is challenging. Temperature modulated DSC methods allow to separate a reversing, time independent, heat flow reflecting the specific heat background from an irreversible kinetic heat flow that may encompass the latent heat. But this technique generally yields a modest accuracy on the specific heat [47–51]. Thermopile calorimeters operated in AC or scanning mode have proved capable of separating specific heat from latent heat in giant magnetocaloric materials such as in CoMnSi compounds [52]. But this method requires homemade instruments and is limited to relatively small samples. We propose a method based on commercial calorimeter to separate latent heat from the total thermal response of the material in (Mn,Fe)₂(P,Si) materials. This investigation led us to establish a correlation between L and another intrinsic quantity, U_e the (magneto-) elastic energy.

Our detailed magnetic and thermal measurements carried out up to high magnetic fields demonstrate that the present materials show a change in the nature of the phase transition when the applied magnetic field causes the transition to reach a critical end point. The reduction of both $\Delta T_{\rm hys}$ and L is gradual with applied magnetic field, and both vanish at the critical end point.

2. Materials and experimental methods

 $Mn_{0.60+x}Fe_{1.3-x}P_{0.66-y}Si_{0.34+y}$ alloys (with x=2y ranging from x=10.00 until x = 0.08) were synthesized by ball milling from powders of high-purity starting materials of Mn (99.7 %), Fe (99.8 %), Fe₂P (99.5 %), and Si (99.6 %), using a ball-to-sample mass ratio of 5:1 and ball milling for 10 h at 380 rpm. Subsequently, the resulting powders were compacted into cylinders of approximately 2.5 g each using an uniaxial press with a force of 8 tons. Then the pellets were melted and quenched by melt spinning with a copper-wheel speed of $v \approx 30$ m/s. Melt spun ribbons with widths of 2-3 mm and a thickness of 20-40 μm were produced. Following this, the samples were sealed in quartz tubes filled with argon gas at a pressure of 200 mbar. Sintering of the samples took place in a vertical furnace, which had been preheated to 1100 °C. This sintering process lasted for 2 h before the samples were quenched in room temperature water. The choice of the sintering temperature of 1100 °C was based on previous studies, which identified it as the optimal temperature for sintering [53,54]. Additionally, for comparative purposes, a ball-milled sample was annealed at the same temperature for 24 h to complement the analysis of differences observed before and after melt spinning.

Powder X-Ray Diffraction (XRD) was carried out on a PANalytical X-Pert PRO diffractometer, using Cu-K $_{\alpha}$ radiation with a wave length of 1.5405 Å (probing an angular range of 10° - 90° , with an angular step of 0.02° , 1 s exposure per step). Temperature-dependent XRD measurements were performed with an Anton Paar TTK450 temperature chamber. The Rietveld method [55], as implemented in the FullProf software, was used for the crystal structure refinement [56].

Scanning electron microscopy (SEM, JEOL JSM-IT800SHL) and energy-disperse X-ray spectroscopy (EDS, Oxford Instruments Ultim Max 100 mm² with Aztec data-acquisition software) was used to characterize the microstructure and the composition. SEM measurements were performed on the free side of the ribbon samples and on eroded surfaces of compacted pellets, using a Nital etchant. For the grain size evaluation, about 15 SEM images per samples were analysed using the MIPAR software [57] for a quantitative estimate of the average grain size.

The temperature- and field-dependent magnetization was measured with a superconducting quantum interference device (Quantum Design MPMS XL) magnetometer, using the reciprocating sample option (RSO). Isofield magnetization curves were recorded as a function of the temperature in sweep mode at a rate of 1.0 K/min.

Heat capacity measurements were performed on a semi-adiabatic heat capacity option of a VersaLab system (Quantum Design) using the built-in "2τ" relaxation method supplemented by an external analysis referred to as Single Pulse Method (SPM) [58,59]. By leveraging the finite thermal hysteresis of the FOMT, we propose using the standard 2τ measurements and analyses performed consecutively at the same bath temperature to insulate the reversible specific heat. This approach assumes that repeatedly performing heat pluses of amplitude significantly smaller than the hysteresis will consume the latent heat in order to get access to the underlying reversible specific heat. It bares certain conceptual features with modulated DSC or amplitude modulated DSC techniques [60], as it allows separating a time- or history- independent specific heat. Contrary to DSC methods usually employing a continuous underlying thermal ramp, our method is based on discrete successive heat pulses. In practice, three consecutive heat pulses of 2 K amplitude (i.e. $< \Delta T_{hyster} \approx 3$ K) were performed. The time evolution of the sample temperature and the influence of the latent heat are illustrated in Fig. S1

(Supplementary Information). During the 1st pulse, the T(t) branch upon heating exhibit a "kink" marking out the heat absorbed as latent heat at $T_c^{heating}$. During the subsequent relaxation process, the sample temperature remains higher than $T_c^{cooling}$, so that the reverse transformation does not occur. The time profile of the next heat pulses performed at the same bath temperature is notably different from the first pulse, and reflects only a reversible specific heat. The latent heat peak is measured by SPM during an independent measurement based on a 7 K heat pulse. Fig. 1 illustrates the method by comparing the third 2τ standard measurements with the SPM. The SPM yields a strong and symmetrical latent heat peak typical of a FOMT with a thermal hysteresis between heating and cooling branches of approximately 3.0 K. As illustrated in Fig. S2 in the supplementary information, using the standard 2τ method, the first heat pulse will contain a partial latent heat contribution (only a partial latent heat contribution due to the thermal stabilisation prior to the pulse and because of the built-in specific heat analysis using both heating and cooling branches [58]). The subsequent pulses carried out at the same bath temperature will not contain latent heat and will thereby reflect the reversible specific heat background (C_{rev}). The latent heat contribution (dL/dT) can then be obtained by subtracting this C_{rev} to the total $C_{\text{rev}}+dL/dT$ measured by SPM.

3. Results and discussion

3.1. Crystal structural information and average crystallite size

The X-ray diffraction patterns at 400 K shown in Fig. 2a confirm that the synthesized $Mn_{0.60+x}Fe_{1.3-x}P_{0.66-y}Si_{0.34+y}$ (0 $\leq x \leq$ 0.08, x = 2y) samples are single phase with the expected hexagonal *P*-62*m* symmetry. As shown in Fig. 2b and c, the lattice parameter a and the unit-cell volume V clearly increase with the increase in Mn and Si contents, whereas the lattice parameter c presents a less significant evolution; as a result, the c/a ratio decrease. The structural refinement parameters obtained from the XRD data are summarized in Table 1. The unit-cell volume expansion is in line with the expectation from Vegard's law and the respective metallic radii of the elements. The temperature evolution of the (300), (211) and (002) powder XRD reflections upon heating is illustrated in Fig. 2d for the Mn_{0.66}Fe_{1.24}P_{0.63}Si_{0.37} compound. The effect of temperature on the unit cell dimensions is presented in Fig. S3 (Supplementary Information). The FM and PM phases show a phase transition centred at $T_{\rm tr}=320$ K with step-like anomalies of: $\Delta a/a=$ -0.98%, $\Delta c/c = 1.88\%$, $\Delta (c/a)/(c/a) = 2.81\%$, $\Delta V/V = 2(\Delta a/a) + \Delta c/a$ $c \approx -0.1$ %, as shown in Fig. S3 (Supplementary Information). The amplitude of the discontinuities in lattice parameters significantly

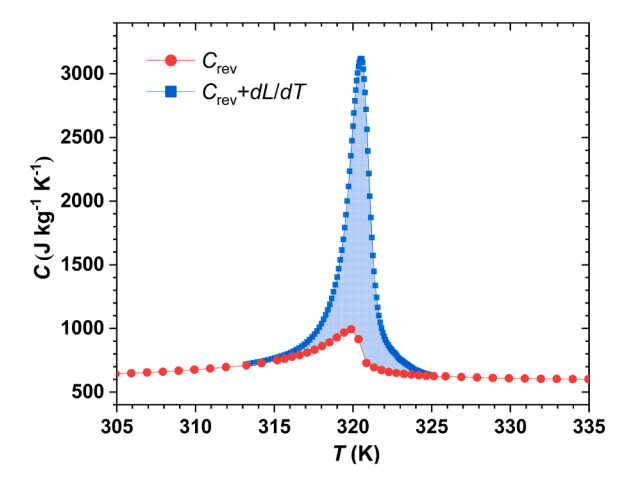


Fig. 1. Heat capacity of $\mathrm{Mn}_{0.66}\mathrm{Fe}_{1.24}\mathrm{P}_{0.63}\mathrm{Si}_{0.37}$ at $\mu_0H=0$, 3rd repetition (closed circles) of the standard " 2τ " method) and SPM (closed squares). The shaded area marks the latent heat.

increase with x, indicating a strengthening of the FOMT. Theoretical calculations have noted that the c/a ratio bears a significant correlation with the magnetic exchange interactions governing the magnetoelastic coupling in Fe₂P-type materials [61,62]. The reduction in c/a with the increase in x is anticipated to result in increasing Curie temperatures.

When comparing the grain size of the hexagonal phase between samples with x = 0.60 and 0.68, no clear trend is observed for a simultaneous increase of Mn and Si contents. As shown in Fig. 3, both samples show a low porosity and a similar log-normal distribution of grain size with an average size of about 8 µm. For bulk (Mn,Fe)2(P,Si) prepared by ball-milling followed by solid state reaction, grain sizes are strongly influenced by the sintering temperature and the annealing time [63]. Considering a typical high-temperature sintering for 24–48 h, the grain size was found to range from about 27 μm in Mn-rich compositions [64] to 24–26 μ m in compositions with a Mn/Fe = 1 ratio [65,66]. In contrast, a comparison of the microstructures of the melt-spun and ball-milled samples shows pronounced differences (see Fig. S4, Supplementary Information). The ball-milled sample exhibits a significant amount of porosity, with a SiO2 impurity phase concentrated at the pores. However, EDS analysis indicates that the overall compositions of the main phase are nearly the same for the two different methods, as show in Table S1 (Supplementary Information). The melt-spinning process therefore offers the advantage of eliminating oxide impurities. Furthermore, the melt-spun ribbons display a significantly smaller average grain size and a finer overall microstructure. This is critical for the stabilization of the mechanical properties, as the reduction in grain size is anticipated to reduce the maximum shear strain at grain boundaries, thereby enhancing the mechanical stability of these materials. In the ribbon samples, thermal cycling induces microcrack initiation at grain boundaries, followed by subsequent propagation into the interior of the grains, as shown in Fig. S5 (Supplementary Information). Using these ribbon samples, we constructed a bulk sample and sintered it at 1100 °C for 24 h. Encouragingly, as shown in Fig. S6 (Supplementary Information), the average grain size remained nearly constant at 8-10 μm , highlighting the potential of shaping bulk samples from ribbon materials.

3.2. Magnetic and magnetocaloric properties

The temperature-dependent magnetization M(T), is shown in Fig. 4a for field-cooling (FC) and field-heating (FH) conditions. The same overall magnetic response with a relatively sharp ferromagnetic FOMT and a finite thermal hysteresis ($\Delta T_{\rm hys}$) is found in all samples. The magnetization curves at 5 K, shown in Fig. 4b, start to saturate in an applied field of 1 T The saturation magnetizations at 5 K and 5 T fall in the range 160–190 Am²kg⁻¹. While in overall agreement with the literature for similar Fe₂P-based compounds [39,67,68], these large saturation magnetization values primarily originate from the high phase purity of the ribbon samples. As expected, the saturation magnetizations tend to increase with the increase in Mn content. However, the evolution does not follow a perfectly linear evolution, which can be attributed to minor compositional variations. According to EDS results (see table S2), the effective compositions can present deviations with respect to the nominal ones; but the overall trend, an increase in effective Mn and Si contents with x, is observed. The transition temperature T_C is estimated from the minimum in the temperature derivative of the magnetization (dM/dT), as shown in the inset of Fig. 4c. T_C increases linearly with the simultaneous increase in Mn and Si concentrations, in line with the c/atrend. The parent compound Mn_{0.6}Fe_{1.3}P_{0.66}Si_{0.34} shows a thermal hysteresis $\Delta T_{\rm hys}$ of about 3 K. The value of $\Delta T_{\rm hys}$ progressively increases with x, yet it remains relatively limited, within 5 K for all compounds (recalling that thermal lags in sweeping conditions overestimate $\Delta T_{\rm hys}$). The origin of the thermal hysteresis can be separated into intrinsic (associated with the mechanism of the transition at atomic scale [7]) and extrinsic contributions related to microstructure; the presence of nano-precipitates [69], micro-cracks [70] or micro-pores [71], strains

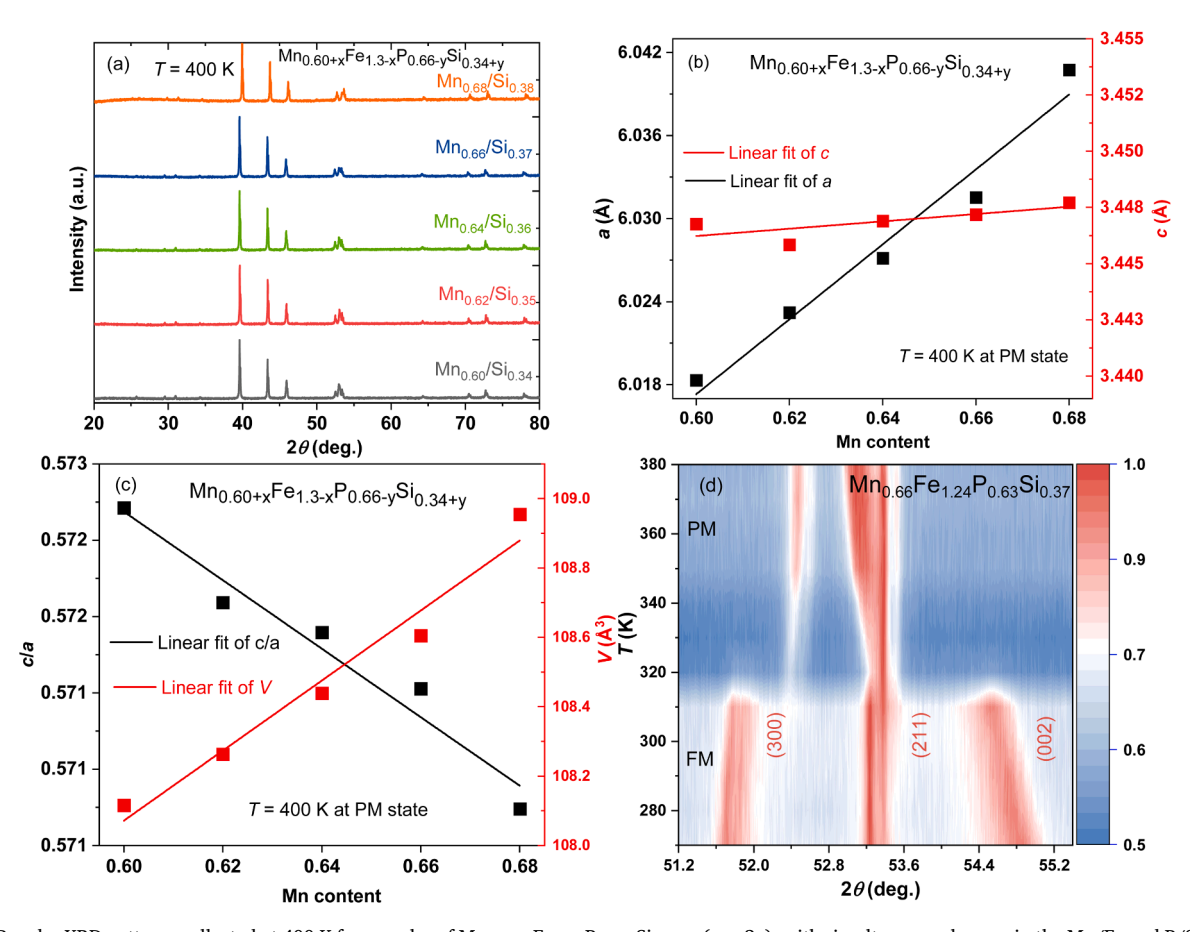


Fig. 2. (a) Powder XRD patterns collected at 400 K for samples of $Mn_{0.60+x}Fe_{1.3-x}P_{0.66-y}Si_{0.34+y}$ (x=2y), with simultaneous changes in the Mn/Fe and P/Si ratios. (b) Lattice parameter a and c, (c) Unit-cell volume V and c/a ratio derived from XRD as a function of the Mn concentration for $Mn_{0.60+x}Fe_{1.3-x}P_{0.66-y}Si_{0.34+y}$ (x=2y). (d) Intensity versus scattering angle 2Θ (°) as a function of temperature T (K) for the $Mn_{0.66}Fe_{1.24}P_{0.63}Si_{0.37}$ compound.

Table 1Lattice parameters a and c, c/a ratio and unit-cell volume V obtained from XRD at 400 K, saturation magnetization M_s and Curie temperature T_C for the $Mn_{0.60+x}Fe_{1.3-x}P_{0.66-y}Si_{0.34+y}(x=2y)$ compounds. M_s is obtained from magnetization measurements at 5 K and the transition temperature T_C is defined as the minimum in dM/dT in an applied field of 0.01T.

| Mn | A (Å) | c (Å) | c/a | V (ų) | $M_{\rm s, 5 \ K@5 \ T}$ (Am ² kg ⁻¹) | T ^{Heating} (K) |
|------|------------|------------|-------------|------------|--|-----------------------------|
| 0.60 | 6.01832(4) | 3.44676(6) | 0.57271(14) | 108.116(3) | 176.56 | 295.3 |
| 0.62 | 6.02322(8) | 3.44584(5) | 0.57209(11) | 108.263(2) | 177.27 | 305.2 |
| 0.64 | 6.02715(9) | 3.44692(5) | 0.5719(11) | 108.439(3) | 185.93 | 312.3 |
| 0.66 | 6.03154(8) | 3.44719(5) | 0.57153(11) | 108.605(3) | 188.70 | 322.1 |
| 0.68 | 6.04076(8) | 3.44771(5) | 0.57074(11) | 108.954(3) | 186.81 | 331.2 |

and stresses at interfaces [7], etc. For instance, recent studies by Suye et al. [65] and Zhang et al. [72] have reported that ΔT_{hys} tends to decrease with a reduction in particle size. Here, the increase in $\Delta T_{\rm hys}$ with x involves an intrinsic contribution from the strengthening of the transition with x as indicated by the increased $\Delta(c/a)$ in Fig. S3 (Supplementary Information) and by the increased latent heat in the next subsection. Furthermore, a comparison of the magnetic properties of the melt-spun and ball-milled samples reveals clear differences in magnetization, the sharpness of the phase transition, and thermal hysteresis (see Fig. S7). The melt spun samples exhibit a higher saturation magnetization, a sharper transition and a lower thermal hysteresis than ball milled samples. These differences can be attributed to the elimination of the SiO₂ phase and microstructural voids, the refinement of the grain size, and the potentially more efficient annealing for ribbon with a limited thickness. These findings suggest that the grain refinement in melt-spun ribbons was beneficial to extrinsically reduce the ΔT_{hys} , which in turn is advantageous for MCE applications.

The magnetocaloric performance expressed as the isothermal entropy change ΔS is shown in Fig. 4d The isothermal entropy change is calculated by applying the Maxwell relation $\Delta S(T)_{\Delta H}=$

$$\int_{H_i}^{H_f} \mu_0 \left(\frac{\partial M(T, H)}{\partial T} \right)_H dH [27,73] \text{ to the isofield } M(T) \text{ data. All samples}$$

show high $|\Delta S|$ values typical for the GMCE observed at the FOMT in Mn_{0.60+x}Fe_{1.3-x}P_{0.66-y}Si_{0.34+y} compounds. The parent compound Mn_{0.6}Fe_{1.3}P_{0.66}Si_{0.34} exhibits $|\Delta S_{\rm max}| = 12~\rm J~kg^{-1}~K^{-1}$ for an applied field change of 2 T The simultaneous increase of Mn and Si concentration increased $|\Delta S_{\rm max}|$ by 40 %. Furthermore, the heating-cooling averaging ΔS method offers an estimate of the reversible $\Delta S_{\rm rev}$, as shown in the inset of Fig. 4d, confirming the possibility to use these large ΔS in applications. The present results demonstrate the achievement of a well-balanced combination of a small hysteresis and a large $|\Delta S_{\rm max}|$ in the Fe-rich Mn-Fe-P-Si without doping with other elements.

To qualitatively evaluate the order of the magnetic phase transition

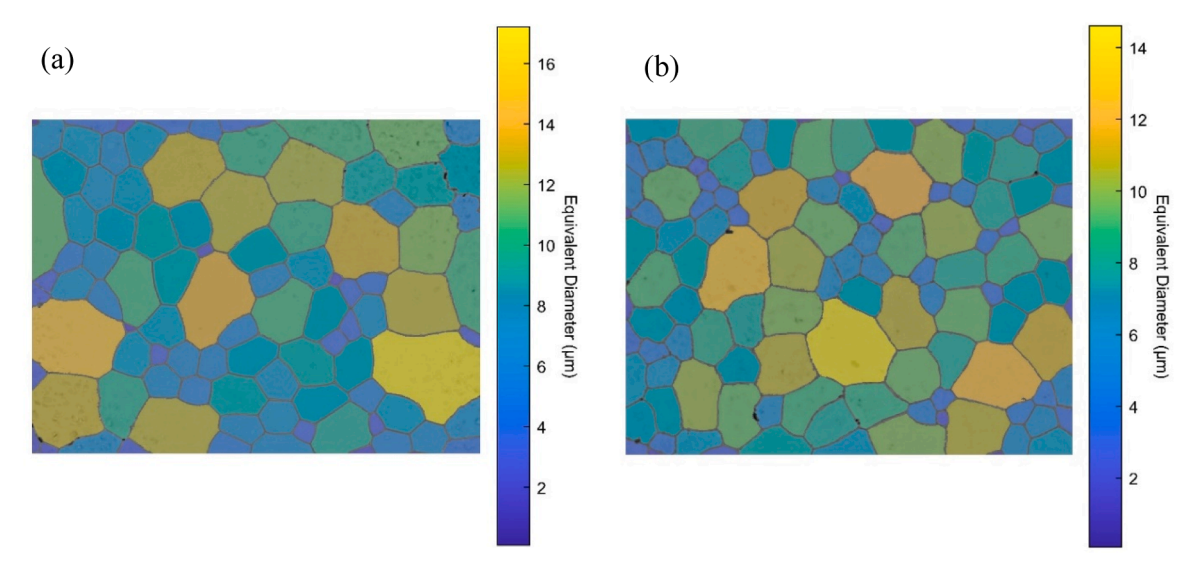


Fig. 3. SEM images of (a) $Mn_{0.60}Fe_{1.30}P_{0.66}Si_{0.34}$ and (b) $Mn_{0.68}Fe_{1.22}P_{0.62}Si_{0.38}$ samples sintered at 1100 °C for 2 h. A colour code highlighting the equivalent diameter of each grain is superposed on the images.

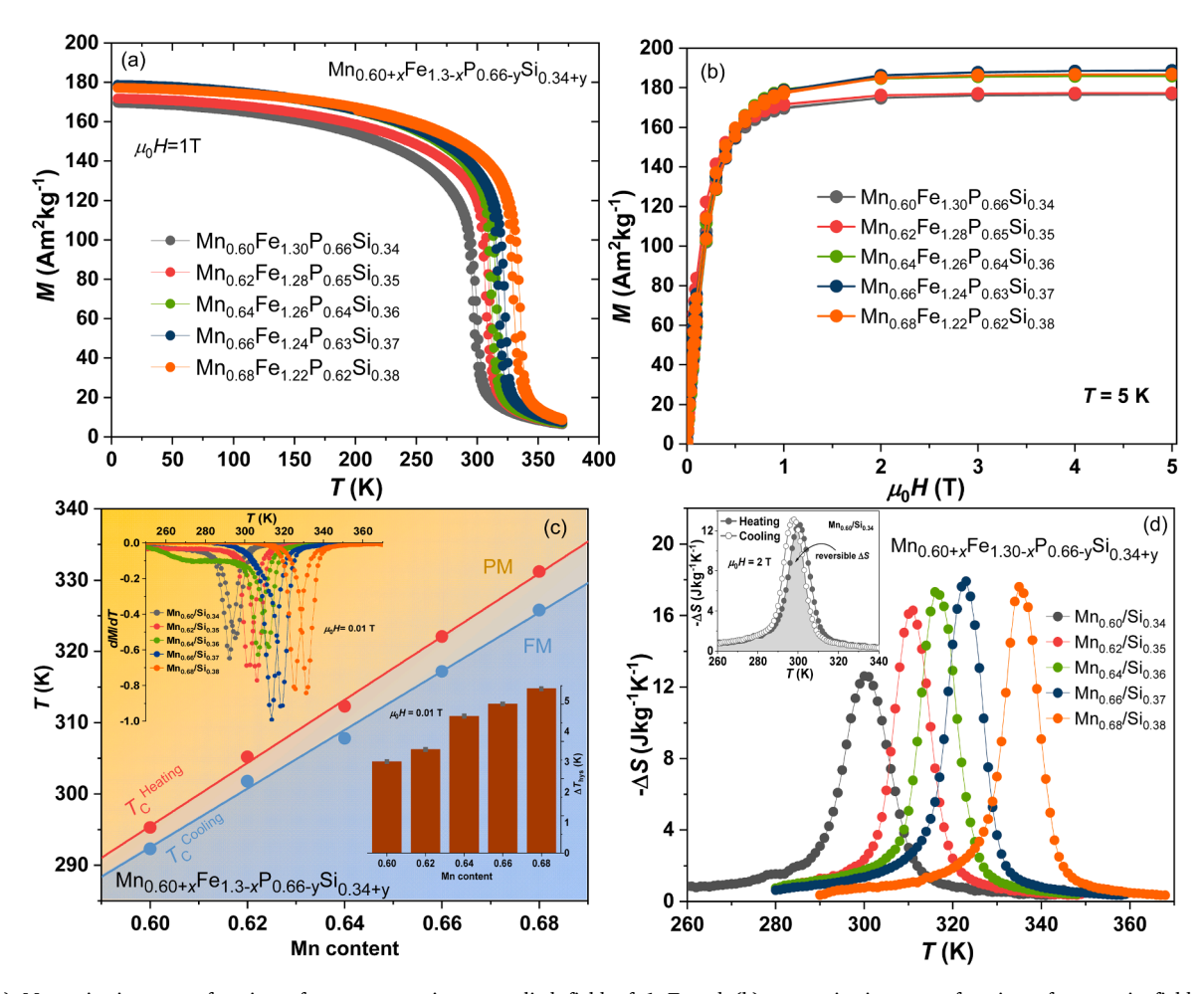


Fig. 4. (a) Magnetization as a function of temperature in an applied field of 1 T and (b) magnetization as a function of magnetic field at 5 K of $Mn_{0.60+x}Fe_{1.3-x}P_{0.66-y}Si_{0.34+y}$ (x=2y). (c) Values of T_{tr} Heating and T_{tr} cooling as a function of the Mn content (inset shows dM/dT curves and thermal hysteresis ΔT_{hys} as a function of the Mn content at an applied field of 0.01T). (d) Isothermal entropy change -ΔS from the temperature-dependent magnetization M(T) upon heating for a magnetic field change of 2 T for $Mn_{0.60+x}Fe_{1.3-x}P_{0.66-y}Si_{0.34+y}$ (x=2y).

in $Mn_{0.60+x}Fe_{1.3-x}P_{0.66-y}Si_{0.34+y}$ compounds the field exponent of the entropy change is examined. As proposed by Franco and coworkers [74, 75] and Van Dijk [76] the field-dependence of the isothermal entropy

change follows a power law of the form $|\Delta S| \propto H^n$. The field exponent n can be employed to determine the FOMT or SOMT nature of the magnetic phase transition. For a FOMT the field exponent has a minimum

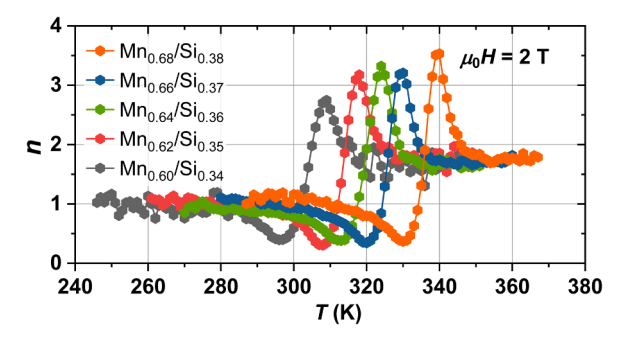


Fig. 5. Field exponent of the isothermal entropy change $n=\frac{dln(|\Delta S|)}{dln(H)}$ for the $Mn_{0.60+x}Fe_{1.3-x}P_{0.66-y}Si_{0.34+y}$ (x=2y) compounds.

value of n=0 and a divergent maximum value $(n\to\infty)$ near the transition [76]. This behavior is due to the step change in entropy (S) associated with the FOMT. In experimental studies, a maximum value of the field exponent n above 2 is taken as indication of a FOMT. Fig. 5 shows the field exponent n of the isothermal entropy change (ΔS) for the $Mn_{0.60+x}Fe_{1.3-x}P_{0.66-y}Si_{0.34+y}$ compounds. The field exponent n is consistently above 2 near T_C for all compounds. This is in line with the observation of finite $\Delta T_{\rm hys}$ and latent heat peaks. Note that the minimum value of n remains above zero near the transition due to the persistence of short-range ferromagnetic fluctuations above T_C .

3.3. Indirect measurements of the giant magnetocaloric effect from specific heat

To evaluate the MCE performance, both the isothermal entropy change (ΔS) and the adiabatic temperature change ($\Delta T_{\rm ad}$) need to be considered. In field specific-heat measurements allow to indirectly evaluate these two quantities. A *S-T* diagram relative to the starting

temperature
$$T_0$$
 can be built, with $S(T,B)$ - $S(T_0,B) = \int\limits_{T}^{T_f} \frac{C_{total}}{T} dT$ for which

 C_{total} contains both the reversible C_{rev} and the latent heat contribution. As illustrated in Fig.6, subtraction between entropy lines at constant entropy or temperature yields ΔT_{ad} and ΔS , respectively. The measurements were caried out for all compositions. Fig. 6 illustrates the case of $Mn_{0.66}Fe_{0.24}P_{0.63}Si_{0.37}$, which is detailed hereafter. An intense specific heat peak with a maximum value of 3.12 Jg⁻¹K⁻¹ is found at 320 K. The maximum value of C_{total} decreases continuously with increasing applied magnetic field. The shift of $T_{\rm tr}$ with the applied magnetic field corresponds to $dT_{\rm tr}/\mu_0 dH \approx 3.9~{\rm K}~{\rm T}^{-1}$, as listed in Table 2. Calorimetric measurements lead to a $|\Delta S_{max}|=16.66~J~kg^{\text{-}1}~K^{\text{-}1}$ at a field change of 2 T well in line with that measured from magnetization data $|\Delta S_{\text{max}}|$ = 17.61 J kg⁻¹ K⁻¹ at a field change of 2 T This agreement confirms that the ΔS data from magnetization measurements were not affected by spike artifacts. Furthermore, a large $\Delta T_{\rm ad}$ of 5.4 K was observed at 2 T Even tough determinations of ΔT_{ad} for (Mn,Fe)₂(P,Si) compounds are scarcer than ΔS [66], the present performances turn out on par or larger than the best performances observed so far. The simultaneously achieved high values of both $|\Delta S_{\text{max}}|$ and ΔT_{ad} underscore the potential of (Mn, Fe)2(P,Si) ribbons for heat pump applications, particularly given the

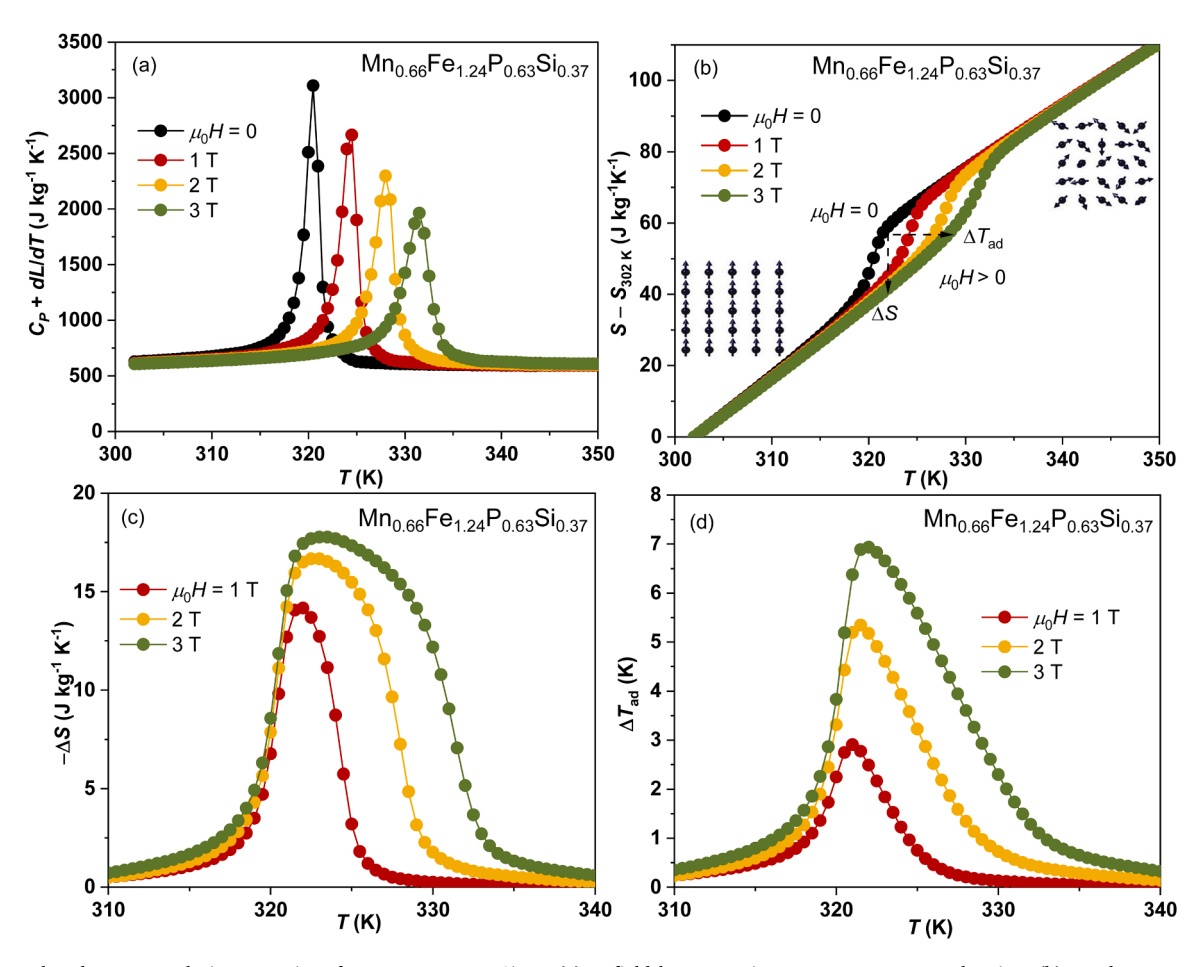


Fig. 6. Thermal and magnetocaloric properties of Mn_{0.66}Fe_{1.24}P_{0.63}Si_{0.37}. (a) In-field heat capacity measurements upon heating. (b) Total entropy versus temperature (*S-T* diagram) in a magnetic field of 0, 1, 2 and 3 T (c) Isothermal entropy change. (d) Adiabatic temperature change from calorimetry measurements.

Table 2 FOMT parameters as a function of the Mn concentration, showing changes in the lattice parameters Δa and Δc at T_C obtained from XRD measurements. The elastic strain energy was calculated from the step changes in lattice parameters observed in XRD vs T at $\mu_0 H = 0$. The isothermal entropy change (at 1 and 2 T), adiabatic temperature change, the field dependence of the transition temperature ($dT_{tr}/\mu_0 dH$), latent heat (L) upon heating by integration of dL/dT data at $\mu_0 H = 0$ and thermal hysteresis were derived from calorimetry measurements.

| Mn | Δα | Δc | $U_{\rm e}$ | $ \Delta S_{max,1\&2T} $ | | $\Delta T_{ad,2T}$ | $dT_{tr}/\mu_0 dH$ | <u>L</u> | ΔT_{hys} |
|-------|------------|-----------|---------------------|--------------------------------------|----------|--------------------|---------------------|---------------------|------------------|
| Units | (Å) | (Å) | (Jg ⁻¹) | (Jkg ⁻¹ K ⁻¹) | _ | (K) | (KT ⁻¹) | (Jg ⁻¹) | (K) |
| 0.60 | -0.0474(2) | 0.0506(1) | 2.49(4) | 6.6(1) | 10.4(2) | 3.6(1) | 3.9(1) | 2.02(2) | 3.0(1) |
| 0.62 | -0.0506(3) | 0.0542(2) | 3.20(5) | 11.6(2) | 15.6(3) | 5.1(1) | 4.0(1) | 3.29(7) | 3.4(1) |
| 0.64 | -0.0526(1) | 0.0580(1) | 3.49(5) | 11.3(2) | 14.0 (3) | 4.8(1) | 4.2(1) | 3.83(8) | 4.5(1) |
| 0.66 | -0.0601(1) | 0.0635(1) | 4.37(7) | 14.2(3) | 16.7(3) | 5.4(1) | 3.9(1) | 4.35(9) | 4.9(1) |
| 0.68 | -0.0648(1) | 0.0689(1) | 5.13(8) | 13.3(3) | 16.6(3) | 5.1(1) | 4.2(1) | 5.79(12) | 5.4(1) |

ability to fine tune the transition temperature above room temperature.

3.4. Correlation of pure latent heat with elastic strain energy

The heat capacity is a basic physical quantity reflecting all degrees of freedom and usually is decomposed into magnetic, structural and electronic terms $C_p^{tot} = C_p^{el} + C_p^{ph} + C_p^{m}$. Each of these terms could be individually estimated outside the FOMT [65], but such a decomposition could not legitimately be carried out at the magneto-elastic transition. Here, one does not seek to separate magnetic, lattice and electronic terms, but rather to quantify the peak-shaped latent heat $(T) \cong Lma(T)$, where G(T) is a normalised Gaussian distribution centred at T_C . Experimentally, this requires a subtraction of the reversible heat capacity (C_{rev}) background from the total specific heat. While this is commonly

done by considering a linear extrapolation in the transition region, here we used the method presented in the method section to determine C_{rev} .

Fig. 7 illustrates the evolution for different magnetic fields of the latent heat contribution to the $\rm Mn_{0.66}Fe_{1.24}P_{0.63}Si_{0.37}$ compound. The latent heat progressively decreases with the increase in magnetic field. A linear extrapolation indicates that it would vanish at a critical field of about 6.4 T The full width at half maximum (FWHM) of the latent heat peak was derived from a Gaussian fit. FWHM progressively increases with the applied magnetic field, indicating a broadening of the transition at higher fields. Complementary magnetization measurements were carried out as a function of temperature and field near the FOMT and a magnetic phase diagram was constructed. The thermal hysteresis $\Delta T_{\rm hys}$ estimated from M(T) curves decreases as the first-order nature of the transition is gradually suppressed by the applied magnetic field, with a

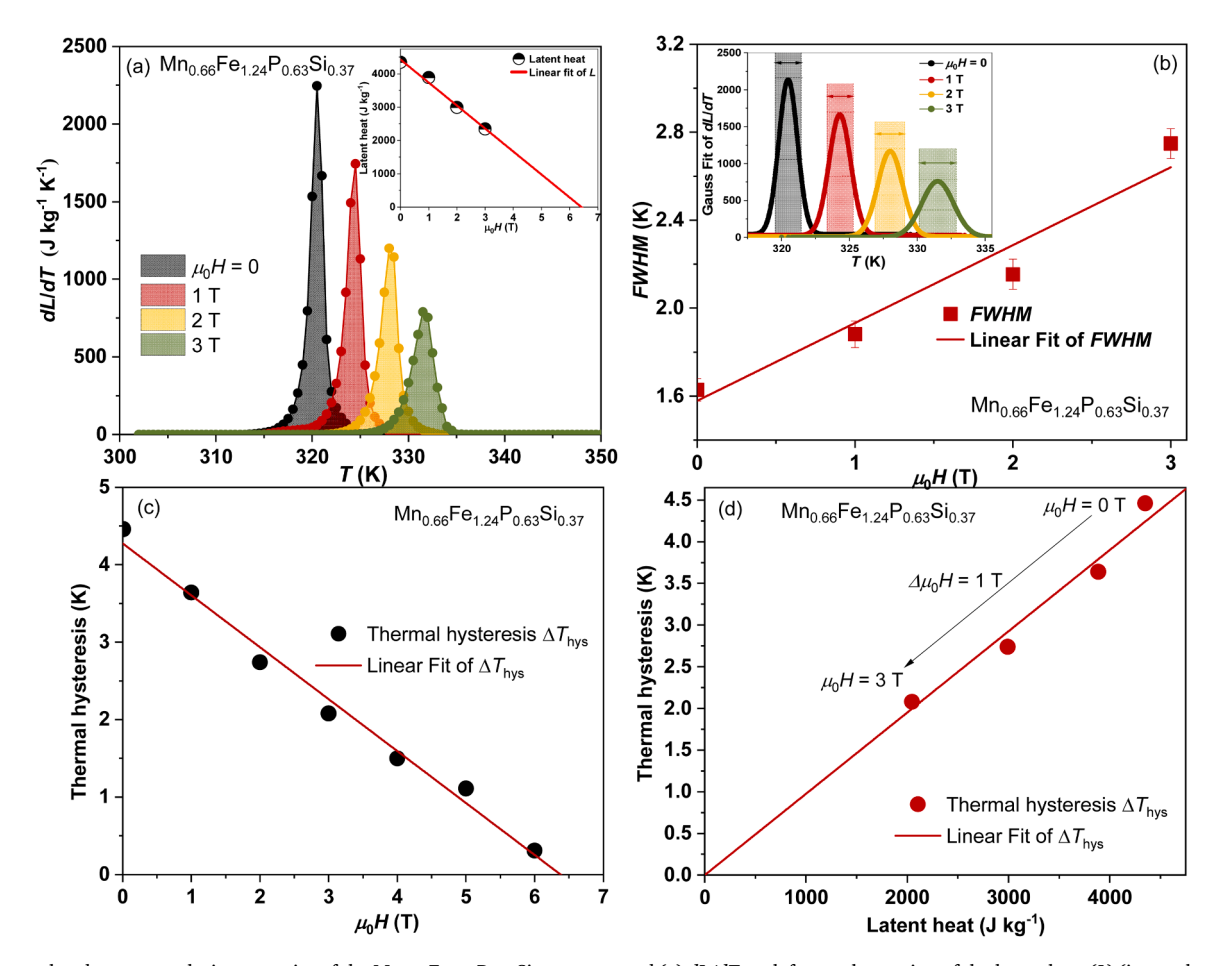


Fig. 7. Thermal and magnetocaloric properties of the $Mn_{0.66}Fe_{1.24}P_{0.63}Si_{0.37}$ compound (a) dL/dT peak from substruction of the latent heat (L) (insert shows an value of L at different magnetic field). (b) Full width at half maximum (FWHM) of the dL/dT peak for recorded in different applied field. (c) Thermal hysteresis (ΔT_{hys}) versus magnetic fields, derived from magnetization measurements, with $\pm 1K/min$ of heating and cooling curves recorded at different applied field. (d) Proportional relation between latent heat (L) and thermal hysteresis (ΔT_{hys}) in the presence of an applied field, as derived from calorimetric and magnetization measurements.

linear extrapolation indicating that $\Delta T_{\rm hys}$ vanishes at 6.4 T, as show in panel 7c of Fig. 7. In the M(H) curves, the field induced transition reveals that the magnetic hysteresis is gradually reduced as temperature increases, with the derivative $dM/d\mu_0H$ suggesting that hysteresis vanishes beyond 6.6 T, as show in Fig. S8c-d (Supplementary Information). Both magnetization and the calorimetric data identify a critical field in the range of 6.4–6.6 T Beyond this critical field, L and $\Delta T_{\rm hys}$ are no longer observable within the experimental resolution. Fig. 7d depicts both L and $\Delta T_{\rm hys}$ at different fields. The apparent correlation suggests that these two parameters are linked.

The latent heat determination was carried out at different applied fields for all compounds, as shown in Fig. 8. The five compositions follow the same trend, indicating that the latent heat L decreases as the applied field increases. Regarding the zero-field latent heat, the simultaneous increase in Mn and Si (with x = 2y) results in an increase in L from $2.02\ J\ g^{-1}$ to $5.79\ J\ g^{-1}$. This result is consistent with the observed increase in $\Delta T_{\rm hys}$ and the trends for the discontinuity of the lattice parameters for increasing Mn and Si concentrations. In former studies [6, 32,67,77,78], attempts were made to establish a relation between various factors involved in the FOMT of Fe₂P-based compounds. Miao et al. [32] proposed the existence of a relation between $\Delta T_{\rm hys}$ and $U_{\rm e}$ for a large range of Fe₂P-based compounds. However, $\Delta T_{\rm hys}$ can hardly be regarded as an intrinsic quantity for the FOMT. A recent report demonstrated a correlation between entropy change at the transition (ΔS_{tr}) and the lattice deformation (c/a ratio) [79]. As these two are intrinsic physical quantities, they provide a more reliable basis for scaling. This prompted us to investigate a possible relation between the latent heat and the elastic strain energy (magneto-elastic coupling). The transition-induced elastic strain energy can be expressed as: U_e $=(C_{11}+C_{12})e_1^2+2C_{13}e_1e_3+C_{33}e_3^2/2$ where e_{ij} represent the tensile strains and C_{ii} correspond to the elastic constants [32,77]. For an hexagonal lattice: $e_1 = e_2 = \Delta a/a$ within the *a-b* plane and $e_3 = \Delta c/c$ along the c axis. For the evaluation of the elastic strain energy we applied the elastic constants from DFT calculations reported by Roy et al. [80] and the experimental elastic strain values for $\Delta a/a$ and $\Delta c/c$ at T_C , as shown in Fig. S3 (Supplementary Information).

A striking proportional relation is observed between L and $U_{\rm e}$, with data points aligning along the diagonal, as shown in Fig. 8b The scaling between intrinsic quantities of L and $U_{\rm e}$ suggests that these quantities are directly related. This correlation indicates that nearly all the latent heat originates from the elastic deformation. For comparison, we reconstructed the elastic strain energy (30.89 kJ kg⁻¹) from previous studies using DFT calculations [81] and found that it is of a similar order of magnitude to the calculated latent heat (19.97 kJ kg⁻¹) for MnFe-Si_{0.33}P_{0.66} compounds, which is line with our present results. To

strengthen the statistical robustness of our analysis, we incorporated experimental results from previous studies on the Fe₂P-compounds [32, 35,82–84]. The latent heat values from previous studies are generally higher than the diagonal in Fig. 8. This difference may be caused by the subtraction of the reversible specific heat in the present study. Using a linear background will underestimate the reversible specific heat near the transition and therefore overestimate the latent heat. Nevertheless, the slope remains consistent, supporting our proposition that a correlation exists between L and U_e . Further experiments are needed to refine these results, in particular to extend the investigations to other (Mn, Fe)₂(P,X) series with X = As, Ge and B while using the present methodology. The present scaling strategy may also be considered for other magnetoelastic FOMT materials, such as La(Fe,Si)₁₃ [21–23], FeRh [24, 25], and Eu₂In [26], where elastic-strain energy similarly impact the first-order magnetic phase transition. (Fig 9).

4. Conclusions

Fe-rich (Mn,Fe)₂(P,Si) ribbons achieve minimal thermal hysteresis, a significant isothermal entropy change and a significant adiabatic temperature change, without the introduction of additional doping elements, making them promising giant magnetocaloric materials. Melt spinning can be used to tailor the microstructure of (Mn,Fe)₂(P,Si)

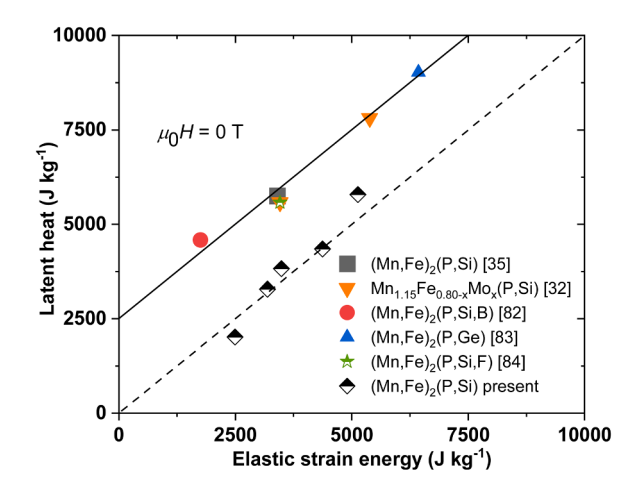


Fig. 9. Latent heat (L) of the FOMT as a function of elastic strain energy (U_e) for the Fe₂P-based system, with the current data compared to reference data from earlier generations of (Mn,Fe)₂(P,Si) compounds, lines are used as guides for the eyes.

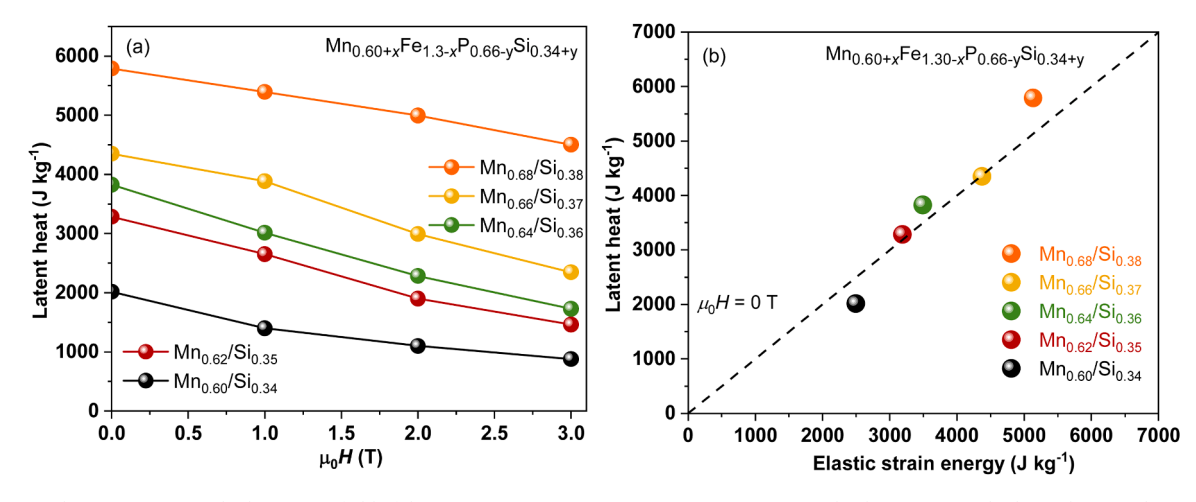


Fig. 8. (a) Latent heat (L) versus applied magnetic field of the Mn_{0.60+x}Fe_{1.3-x}P_{0.66-y}Si_{0.34+y} (x = 2y) compounds. (b) Proportional relation between latent heat (L) and elastic strain energy (U_e) of the FOMT in the Mn_{0.60+x}Fe_{1.3-x}P_{0.66-y}Si_{0.34+y} (x = 2y) compounds.

alloys. We also demonstrate the possibility to shape high-performance bulk samples from ribbon precursors. A comparison between meltspun ribbons and samples prepared by ball-milling indicates significant differences in magnetization and on the sharpness of the phase transition. Additionally, grain refinement in melt-spun ribbons contributes to an extrinsic reduction of ΔT_{hys} . By performing two types of calorimetry measurements to separate the latent heat from reversible heat capacity and quantifying the elastic transformation strain energy by XRD, we establish a direct correlation between the latent heat (L) and the elastic transformation strain energy (Ue) in the (Mn,Fe)2(P,Si) family. The application of an external magnetic field is found to gradually weaken the first-order character of the transition, with both L and $\Delta T_{\rm hvs}$ decreasing and disappearing simultaneously at a critical end point. Generally, achieving a GMCE requires a sizable latent heat, which is inherently accompanied by significant lattice deformations that can introduce undesirable effects, such as thermal hysteresis and mechanical embrittlement. By tailoring the microstructure, melt-spinning offers an approach to break the circle.

CRediT authorship contribution statement

W. Hanggai: Writing – original draft, Visualization, Investigation, Formal analysis. H. Yibole: Investigation. F. Guillou: Writing – review & editing, Investigation. C. Kwakernaak: Investigation. N.H. van Dijk: Writing – review & editing, Supervision. E. Brück: Writing – review & editing, Supervision.

Declaration of competing interest

I have declared that there is no conflict of interest in our work. And in the text box, all other authors have declared that there are no known competing financial interests or personal relationships.

Acknowledgements

The authors thank Anton Lefering, Bert Zwart, Sebastian Couweleers, and Robert Dankelman for their technical assistance. This work is financially supported by the Dutch Research Council NWO TTW with Project no. 17877 and RSP Technology. H. Yibole and F. Guillou acknowledge the support from the National Natural Science Foundation of China (grant n° 12464015 and 52461036).

Supplementary materials

Supplementary material associated with this article can be found, in the online version, at doi:10.1016/j.actamat.2025.121677.

References

- O. Tegus, E. Brück, K.H.J. Buschow, F.R. De Boer, Transition-metal-based magnetic refrigerants for room temperature applications, Nature 415 (2002) 150–152, https://doi.org/10.1038/415150a.
- [2] E. Brück, O. Tegus, D.T.C. Thanh, K.H.J. Buschow, Magnetocaloric refrigeration near room temperature (invited), J. Magn. Magn. Mater. 310 (2007) 2793–2799, https://doi.org/10.1016/j.jmmm.2006.10.1146.
- [3] J.D. Moore, K. Morrison, K.G. Sandeman, M. Katter, L.F. Cohen, Reducing extrinsic hysteresis in first-order La(Fe,Co,Si)₁₃ magnetocaloric systems, Appl. Phys. Lett. 95 (2009) 252504, https://doi.org/10.1063/1.3276565.
- [4] N.H. Dung, Z.Q. Ou, L. Caron, L. Zhang, D.T.C. Thanh, G.A. De Wijs, R.A. De Groot, K.H.J. Buschow, E. Brück, Mixed magnetism for refrigeration and energy conversion, Adv. Energy Mater. 1 (2011) 1215–1219, https://doi.org/10.1002/ aenm.201100252.
- [5] F. Guillou, G. Porcari, H. Yibole, N. van Dijk, E. Brück, Taming the first-order transition in giant magnetocaloric materials, Adv. Mater. 26 (2014) 2671–2675, https://doi.org/10.1002/adma.201304788.
- [6] N.H. Dung, L. Zhang, Z.Q. Ou, E. Brück, Magnetoelastic coupling and magnetocaloric effect in hexagonal Mn–Fe–P–Si compounds, Scr. Mater. 67 (2012) 975–978, https://doi.org/10.1016/j.scriptamat.2012.08.036.
- [7] O. Gutfleisch, T. Gottschall, M. Fries, D. Benke, I. Radulov, K.P. Skokov, H. Wende, M. Gruner, M. Acet, P. Entel, M. Farle, Mastering hysteresis in magnetocaloric

- materials, Phil. Trans. R. Soc. A. 374 (2016) 20150308, https://doi.org/10.1098/rsta-2015-0308
- [8] T. Gottschall, K.P. Skokov, M. Fries, A. Taubel, I. Radulov, F. Scheibel, D. Benke, S. Riegg, O. Gutfleisch, Making a cool choice: the materials library of magnetic refrigeration, Adv. Energy Mater. 9 (2019) 1901322, https://doi.org/10.1002/ aenm 201901322
- [9] V. Franco, J.S. Blázquez, J.J. Ipus, J.Y. Law, L.M. Moreno-Ramírez, A. Conde, Magnetocaloric effect: from materials research to refrigeration devices, Prog. Mater. Sci. 93 (2018) 112–232. https://doi.org/10.1016/j.pmatsci.2017.10.005.
- [10] V. Zverev, A.M. Tishin, Magnetocaloric effect: from theory to practice. Reference Module in Materials Science and Materials Engineering, Elsevier, 2016 B9780128035818028137, https://doi.org/10.1016/B978-0-12-803581-8.02813-7
- [11] K.P. Skokov, A.Yu. Karpenkov, D.Yu. Karpenkov, O. Gutfleisch, The maximal cooling power of magnetic and thermoelectric refrigerators with La(FeCoSi)₁₃ alloys, J. Appl. Phys. 113 (2013) 17A945, https://doi.org/10.1063/1.4801424
- [12] M.F.J. Boeije, P. Roy, F. Guillou, H. Yibole, X.F. Miao, L. Caron, D. Banerjee, N. H. Van Dijk, R.A. De Groot, E. Brück, Efficient room-temperature cooling with magnets, Chem. Mater. 28 (2016) 4901–4905, https://doi.org/10.1021/acs.chemmater.6b00518.
- [13] J. Lyubina, Magnetocaloric materials for energy efficient cooling, J. Phys. D: Appl. Phys. 50 (2017) 053002, https://doi.org/10.1088/1361-6463/50/5/053002.
- [14] A. Kitanovski, Energy applications of magnetocaloric materials, Adv. Energy Materials 10 (2020) 1903741, https://doi.org/10.1002/aenm.201903741.
- [15] C. Zimm, A. Boeder, B. Mueller, K. Rule, S.L. Russek, The evolution of magnetocaloric heat-pump devices, MRS Bull. 43 (2018) 274–279, https://doi.org/ 10.1557/mrs.2018.71
- [16] E. Brück, H. Yibole, V.T. Nguyen, X.F. Miao, M. Boeije, N. Van Dijk, Transition metal based magneto caloric materials for energy efficient heat pumps, SSP 257 (2016) 129–134, https://doi.org/10.4028/www.scientific.net/SSP.257.129.
- [17] E. Brück, Yibole H, L. Zhang, A universal metric for ferroic energy materials, Phil. Trans.R.Soc 374 (2025) 20150303, https://doi.org/10.1098/rsta.2015.0303. A.
- [18] D.J. Silva, J.S. Amaral, V.S. Amaral, Cooling by sweeping: a new operation method to achieve ferroic refrigeration without fluids or thermally switchable components, INT. J. REFRIG. 101 (2019) 98–105, https://doi.org/10.1016/j. iirefrie.2019.02.029.
- [19] R.A. Kishore, S. Priya, A review on design and performance of thermomagnetic devices, Renew. Sustain. Energy Rev. 81 (2018) 33, https://doi.org/10.1016/j. rser.2017.07.035, 44.
- [20] A. Waske, D. Dzekan, K. Sellschopp, D. Berger, A. Stork, K. Nielsch, S. Fähler, Energy harvesting near room temperature using a thermomagnetic generator with a pretzel-like magnetic flux topology, Nat. Energy 4 (2018) 68–74, https://doi.org/ 10.1038/s41560-018-0306-x.
- [21] F. Hu, B. Shen, J. Sun, Z. Cheng, G. Rao, X. Zhang, Influence of negative lattice expansion and metamagnetic transition on magnetic entropy change in the compound LaFe_{11.4}Si_{1.6}, Appl. Phys. Lett. 78 (2001) 3675–3677, https://doi.org/ 10.1063/1.1375836.
- [22] F.X. Hu, L. Chen, J. Wang, L.F. Bao, J.R. Sun, B.G. Shen, Particle size dependent hysteresis loss in La_{0.7}Ce_{0.3}Fe_{11.6}Si_{1.4}C_{0.2} first-order systems, Appl. Phys. Lett. 100 (2012) 072403, https://doi.org/10.1063/1.3684244.
- [23] E. Lovell, A.M. Pereira, A.D. Caplin, J. Lyubina, L.F. Cohen, Dynamics of the first-order metamagnetic transition in magnetocaloric La(Fe,Si)₁₂: reducing hysteresis, Adv. Energy Mater. 5 (2015) 1401639, https://doi.org/10.1002/aenm.201401639.
- [24] G. Li, R. Medapalli, J.H. Mentink, R.V. Mikhaylovskiy, T.G.H. Blank, S.K.K. Patel, A.K. Zvezdin, Th. Rasing, E.E. Fullerton, A.V. Kimel, Ultrafast kinetics of the antiferromagnetic-ferromagnetic phase transition in FeRh, Nat. Commun. 13 (2022) 2998, https://doi.org/10.1038/s41467-022-30591-2.
- [25] A. Aubert, K. Skokov, G. Gomez, A. Chirkova, I. Radulov, F. Wilhelm, A. Rogalev, H. Wende, O. Gutfleisch, K. Ollefs, Simultaneous multi-property probing during magneto-structural phase transitions: an element-specific and macroscopic hysteresis characterization at ID12 of the ESRF, IEEE Trans. Instrum. Meas. 71 (2022) 1–9, https://doi.org/10.1109/TIM.2022.3157001.
- [26] F. Guillou, A.K. Pathak, D. Paudyal, Y. Mudryk, F. Wilhelm, A. Rogalev, V. K. Pecharsky, Non-hysteretic first-order phase transition with large latent heat and giant low-field magnetocaloric effect, Nat. Commun. 9 (2018) 2925, https://doi.org/10.1038/s41467-018-05268-4.
- [27] V.K. Pecharsky, K.A. Gschneidner, Giant magnetocaloric effect in Gd₅(Si₂Ge₂), Phys. Rev. Lett. 78 (1997) 4494–4497, https://doi.org/10.1103/ Phys. Revl. ett. 78 (4994)
- [28] T. Krenke, E. Duman, M. Acet, E.F. Wassermann, X. Moya, L. Mañosa, A. Planes, Inverse magnetocaloric effect in ferromagnetic Ni-Mn-Sn alloys, Nat. Mater. 4 (2005) 450-454, https://doi.org/10.1038/nmat1395.
- [29] W. Hanggai, O. Tegus, H. Yibole, F. Guillou, Structural and magnetic phase diagrams of MnFe_{0.6}Ni_{0.4}(Si,Ge) alloys and their giant magnetocaloric effect probed by heat capacity measurements, J. Magn. Magn. Mater. 494 (2020) 165785, https://doi.org/10.1016/j.jmmm.2019.165785.
- [30] E. Liu, W. Wang, L. Feng, W. Zhu, G. Li, J. Chen, H. Zhang, G. Wu, C. Jiang, H. Xu, F. De Boer, Stable magnetostructural coupling with tunable magnetoresponsive effects in hexagonal ferromagnets, Nat. Commun. 3 (2012) 873, https://doi.org/10.1038/ncomms1868
- [31] K. Mandal, D. Pal, N. Scheerbaum, J. Lyubina, O. Gutfleisch, Magnetocaloric effect in Ni–Mn–Ga alloys, IEEE Trans. Magn. 44 (2008) 2993–2996, https://doi.org/ 10.1109/TMAG.2008.2002481
- [32] X. Miao, Y. Gong, F. Zhang, Y. You, L. Caron, F. Qian, W. Guo, Y. Zhang, Y. Gong, F. Xu, N. Van Dijk, E. Brück, Enhanced reversibility of the magnetoelastic transition

- in (Mn,Fe)₂(P,Si) alloys via minimizing the transition-induced elastic strain energy, J. Mater. Sci. Technol. 103 (2022) 165–176, https://doi.org/10.1016/j.impt.2021.05.087
- [33] Z.Q. Ou, L. Zhang, N.H. Dung, L. Van Eijck, A.M. Mulders, M. Avdeev, N.H. Van Dijk, E. Brück, Neutron diffraction study on the magnetic structure of Fe₂P-based Mn_{0.66}Fe_{1.29}P_{1-x}Si_x melt-spun ribbons, J. Magn. Magn. Mater. 340 (2013) 80–85, https://doi.org/10.1016/j.immm.2013.03.028.
- [34] N.H. Dung, L. Zhang, Z.Q. Ou, L. Zhao, L. Van Eijck, A.M. Mulders, M. Avdeev, E. Suard, N.H. Van Dijk, E. Brück, High/low-moment phase transition in hexagonal Mn-Fe-P-Si compounds, Phys. Rev. B 86 (2012) 045134, https://doi.org/10.1103/ PhysRevB.86.045134.
- [35] F. Guillou, H. Yibole, N.H. Van Dijk, L. Zhang, V. Hardy, E. Brück, About the mechanical stability of MnFe(P,Si,B) giant-magnetocaloric materials, J. Alloys Compd. 617 (2014) 569–574, https://doi.org/10.1016/j.jallcom.2014.08.061.
- [36] Z.Q. Ou, N.H. Dung, L. Zhang, L. Caron, E. Torun, N.H. Van Dijk, O. Tegus, E. Brück, Transition metal substitution in Fe₂P-based MnFe_{0.95}P_{0.50}Si_{0.50} magnetocaloric compounds, J. Alloys Compd. 730 (2018) 392–398, https://doi. org/10.1016/j.jallcom.2017.09.315.
- [37] J. Lai, B. Huang, X. Miao, N. Van Thang, X. You, M. Maschek, L. Van Eijck, D. Zeng, N. Van Dijk, E. Brück, Combined effect of annealing temperature and vanadium substitution for mangetocaloric Mn_{1.2-x}V_xFe_{0.75}P_{0.5}Si_{0.5} alloys, J. Alloys Compd. 803 (2019) 671–677, https://doi.org/10.1016/j.jallcom.2019.06.239.
- [38] S. Hu, X. Miao, J. Liu, Z. Ou, M. Cong, O. Haschuluu, Y. Gong, F. Qian, Y. You, Y. Zhang, F. Xu, E. Brück, Small hysteresis and giant magnetocaloric effect in Nb-substituted (Mn,Fe)₂(P,Si) alloys, Intermetallics 114 (2019) 106602, https://doi.org/10.1016/j.intermet.2019.106602.
- [39] F. Zhang, I. Batashev, N. Van Dijk, E. Brück, Effect of off-stoichiometry and Ta doping on Fe-rich (Mn,Fe)₂(P,Si) based giant magnetocaloric materials, Scr. Mater. 226 (2023) 115253, https://doi.org/10.1016/j.scriptamat.2022.115253.
- [40] F. Zhang, P. Feng, A. Kiecana, Z. Wu, Z. Bai, W. Li, H. Chen, W. Yin, X. Yan, F. Ma, N.H. Van Dijk, E. Brück, Yang Ren, Achieving tunable high-performance giant magnetocaloric effect in hexagonal Mn-Fe-P-Si materials through different D-block doping, Adv. Funct. Mater. (2024) 2409270, https://doi.org/10.1002/adfm.202409270.
- [41] D.M. Liu, H. Zhang, S.B. Wang, W.Q. Xiao, Z.L. Zhang, N. Tian, C.X. Liu, M. Yue, Q. Z. Huang, J.X. Zhang, J.W. Lynn, The effect of Al doping on the crystal structure and magnetocaloric behavior of Mn_{1.2}Fe_{0.8}P_{1-x}Ge_x compounds, J. Alloys Compd. 633 (2015) 120–126, https://doi.org/10.1016/j.jallcom.2015.01.141.
- [42] D.T. Cam Thanh, E. Brück, O. Tegus, J.C.P. Klaasse, K.H.J. Buschow, Influence of Si and Ge on the magnetic phase transition and magnetocaloric properties of MnFe(P, Si,Ge), J. Magn. Magn. Mater. 310 (2007) e1012–e1014, https://doi.org/10.1016/j.immm.2006.11.194.
- [43] P. Wlodarczyk, L. Hawelek, M. Kowalczyk, M. Kaminska, P. Zackiewicz, M. Polak, M. Hreczka, A. Kolano-Burian, Impact of silicon doping on the magnetocaloric effect of MnFeP_{0.35}As_{0.65} powder, Solid State Sci. 56 (2016) 23–28, https://doi.org/10.1016/j.solidstatesciences.2016.04.003.
- [44] S. Kim, H. Shin, I. Chu, K. Lee, K.H. Lee, W. Lee, Tunable Curie temperature in Mn_{1.15}Fe_{0.85}P_{0.55}Si_{0.45} via lattice engineering by Al addition, J. Alloys Compd. 890 (2022) 161798, https://doi.org/10.1016/j.jallcom.2021.161798.
- [45] H. Yibole, F. Guillou, L. Zhang, N.H. Van Dijk, E. Brück, Direct measurement of the magnetocaloric effect in MnFe(P,X) (X=As,Ge,Si) materials, J. Phys. D: Appl. Phys. 47 (2014) 075002, https://doi.org/10.1088/0022-3727/47/7/075002.
- [46] Z.Q. Ou, L. Zhang, N.H. Dung, L. Caron, E. Brück, Structure, magnetism and magnetocalorics of Fe-rich (Mn,Fe)_{1.98}P_{1.98}P_{1.98}Si_x melt-spun ribbons, J. Alloys Compd. 710 (2017) 446–451, https://doi.org/10.1016/j.jallcom.2017.03.266.
- [47] B. Wunderlich, A. Boller, I. Okazaki, K. Ishikiriyama, Heat-capacity determination by temperature-modulated DSC and its separation from transition effects, Thermochim Acta (1997) 125–136, https://doi.org/10.1016/S0040-6031(97) 00184-6, 304–305.
- [48] J.E.K. Schawe, T. Hütter, C. Heitz, I. Alig, D. Lellinger, Stochastic temperature modulation: a new technique in temperature-modulated DSC, Thermochim Acta 446 (2006) 147–155, https://doi.org/10.1016/j.tca.2006.01.031.
- [49] P. Claudy, J.M. Vignon, Temperature modulated DSC theoretical explanation interpretation, J. Therm. Anal. Calorim. 60 (2000) 333–343, https://doi.org/ 10.1023/A;1010148200201.
- [50] S.L. Simon, Temperature-modulated differential scanning calorimetry: theory and application, Thermochim Acta 374 (2001) 55–71, https://doi.org/10.1016/S0040-6031(01)00493-2
- [51] R.L. Danley, New modulated DSC measurement technique, Thermochim Acta 402 (2003) 91–98, https://doi.org/10.1016/S0040-6031(02)00541-5.
- [52] Y. Miyoshi, K. Morrison, J.D. Moore, A.D. Caplin, L.F. Cohen, Heat capacity and latent heat measurements of CoMnSi using a microcalorimeter, Rev. Scientif. Instruments 79 (2008) 074901, https://doi.org/10.1063/1.2960556.
- [53] N.V. Thang, H. Yibole, N.H. Van Dijk, E. Brück, Effect of heat treatment conditions on MnFe(P,Si,B) compounds for room-temperature magnetic refrigeration, J. Alloys Compd. 699 (2017) 633–637, https://doi.org/10.1016/j. iallcom.2016.12.402.
- [54] F. Guillou, O.Haschuluu Sun-Liting, Z.Q. Ou, E. Brück, O. Tegus, H. Yibole, Room temperature magnetic anisotropy in Fe₂P-type transition metal based alloys, J. Alloys Compd. 800 (2019) 403–411, https://doi.org/10.1016/j. jallcom.2019.05.327.
- [55] H.M. Rietveld, The Rietveld method, Phys. Scr. 89 (2014) 098002, https://doi.org/ 10.1088/0031-8949/89/9/098002.
- [56] J. Rodríguez-Carvajal, Recent advances in magnetic structure determination by neutron powder diffraction, Physica B: Condensed Matter 192 (1993) 55–69, https://doi.org/10.1016/0921-4526(93)90108-I.

- [57] J.M. Sosa, D.E. Huber, B. Welk, H.L. Fraser, Development and application of MIPARTM: a novel software package for two- and three-dimensional microstructural characterization, Integr. Mater. Manuf. Innov. 3 (2014) 123–140, https://doi.org/10.1186/2193-9772-3-10.
- [58] V. Hardy, Y. Bréard, C. Martin, Derivation of the heat capacity anomaly at a first-order transition by using a semi-adiabatic relaxation technique, J. Phys.: Condens. Matter 21 (2009) 075403, https://doi.org/10.1088/0953-8984/21/7/075403.
- [59] F. Guillou, R. Hamane, H. Yibole, J.Y. Xu, B. Narsu, V. Hardy, Heat capacity of a MnFe(P,Si,B) compound with first-order magnetic transition, J. Magn. Magn. Mater. 541 (2022) 168513, https://doi.org/10.1016/j.jmmm.2021.168513.
- [60] F.J. Romero, M.C. Gallardo, J.-M. Martín-Olalla, J. Del Cerro, Experimental method to determine specific heat capacity and transition enthalpy at a first-order phase transition: fundamentals and application to a Ni-Mn-In Heusler alloy, Thermochim Acta 706 (2021) 179053, https://doi.org/10.1016/j. tea.2021.179053
- [61] E.K. Delczeg-Czirjak, Z. Gercsi, L. Bergqvist, O. Eriksson, L. Szunyogh, P. Nordblad, B. Johansson, L. Vitos, Magnetic exchange interactions in B-, Si-, and As-doped Fe₂P from first-principles theory, Phys. Rev. B 85 (2012) 224435, https://doi.org/ 10.1103/PhysRevB.85.224435.
- [62] Z. Gercsi, E.K. Delczeg-Czirjak, L. Vitos, A.S. Wills, A. Daoud-Aladine, K. G. Sandeman, Magnetoelastic effects in doped Fe₂P, Phys. Rev. B 88 (2013) 024417, https://doi.org/10.1103/PhysRevB.88.024417.
- [63] T. Qianbai, H. Yibole, F. Guillou, Structure, microstructure and magnetocaloric/ thermomagnetic properties at the early sintering of MnFe(P,Si,B) compounds, Metals 14 (2024) 385, https://doi.org/10.3390/met14040385.
- [64] M. Fries, L. Pfeuffer, E. Bruder, T. Gottschall, S. Ener, L.V.B. Diop, T. Gröb, K. P. Skokov, O. Gutfleisch, Microstructural and magnetic properties of Mn-Fe-P-Si (Fe₂P-type) magnetocaloric compounds, Acta Mater. 132 (2017) 222–229, https://doi.org/10.1016/j.actamat.2017.04.040.
- [65] B. Suye, H. Yibole, W. Meijuan, B. Wurentuya, F. Guillou, Influence of the particle size on a MnFe(P,Si,B) compound with giant magnetocaloric effect, AIP Adv. 13 (2023) 025203, https://doi.org/10.1063/9.0000371.
- [66] B. Suye, H. Yibole, Z.Q. Song, B. Tana, W. Wei, O. Haschuluu, O. Tegus, F. Guillou, Influence of cold compaction pressure on intergranular secondary phase distribution and magnetocaloric/thermomagnetic performances of MnFe(P,Si,B) compounds, J. Alloys Compd. 976 (2024) 172918, https://doi.org/10.1016/j. iallcom.2023.172918.
- [67] A. Kiecana, I. Batashev, A.I. Dugulan, C. Kwakernaak, L. Pieter, F. Zhang, N.H. Van Dijk, E. Brück, Effect of Co and Ni doping on the structure, magnetic and magnetocaloric properties of Fe-rich (Mn,Fe)₂(P,Si) compounds, J. Magn. Magn. Mater. 561 (2022) 169710, https://doi.org/10.1016/j.jmmm.2022.169710.
- [68] A. Kiecana, C. Kwakernaak, N.H. Van Dijk, E. Brück, Effect of the heat treatment on the microstructure, magnetism and magnetocaloric effect in Fe-rich (Mn,Fe) (P,Si) melt-spun ribbons, J. Alloys Compd. 932 (2023) 167635, https://doi.org/10.1016/ i.iallcom.2022.167635.
- [69] R. Niemann, S. Hahn, A. Diestel, A. Backen, L. Schultz, K. Nielsch, M.F.-X. Wagner, S. Fähler, Reducing the nucleation barrier in magnetocaloric Heusler alloys by nanoindentation, APL Mater. 4 (2016) 064101, https://doi.org/10.1063/ 1.4943289.
- [70] A. Waske, L. Giebeler, B. Weise, A. Funk, M. Hinterstein, M. Herklotz, K. Skokov, S. Fähler, O. Gutfleisch, J. Eckert, Asymmetric first-order transition and interlocked particle state in magnetocaloric La(Fe,Si)₁₃, Phys. Status Solidi RRL 9 (2) (2015) 136–140, https://doi.org/10.1002/pssr.201409484.
- [71] J. Lyubina, R. Schäfer, N. Martin, L. Schultz, O. Gutfleisch, Novel design of La(Fe, Si)₁₃ alloys towards high magnetic refrigeration performance, Advan. Mater. 22 (2010) 3735–3739, https://doi.org/10.1002/adma.201000177.
- [72] F. Zhang, C. Taake, B. Huang, X. You, H. Ojiyed, Q. Shen, I. Dugulan, L. Caron, N. H. van Dijk, E. Brück, Magnetocaloric effect in the (Mn,Fe)₂(P,Si) system: from bulk to nano, Acta Mater 224 (2022) 117532, https://doi.org/10.1016/j.actamat.2021.117532.
- [73] K.A. GschneidnerJr, V.K. Pecharsky, A.O. Tsokol, Recent developments in magnetocaloric materials, Rep. Prog. Phys. 68 (2005) 1479–1539, https://doi.org/ 10.1088/0034-4885/68/6/R04
- [74] V. Franco, J.S. Blázquez, A. Conde, Field dependence of the magnetocaloric effect in materials with a second order phase transition: a master curve for the magnetic entropy change, Appl. Phys. Lett. 89 (2006) 222512, https://doi.org/10.1063/ 1.2300361
- [75] J.Y. Law, V. Franco, L.M. Moreno-Ramírez, A. Conde, D.Y. Karpenkov, I. Radulov, K.P. Skokov, O. Gutfleisch, A quantitative criterion for determining the order of magnetic phase transitions using the magnetocaloric effect, Nat. Commun. 9 (2018) 2680, https://doi.org/10.1038/s41467-018-05111-w.
- [76] N.H. Van Dijk, Landau model evaluation of the magnetic entropy change in magnetocaloric materials, J. Magn. Magn. Mater. 529 (2021) 167871, https://doi. org/10.1016/j.jmmm.2021.167871.
- [77] M. Maschek, X. You, M.F.J. Boeije, D. Chernyshov, N.H. Van Dijk, E. Brück, Charge redistribution and the magnetoelastic transition across the first-order magnetic transition in (Mn,Fe)₂(P,Si,B), Phys. Rev. B 98 (2018) 224413, https://doi.org/ 10.1103/PhysRevB 98 224413
- [78] X. You, M. Maschek, N.H.H. Van Dijk, E. Brück, Magnetic phase diagram of the Mn_xFe_{2x}P_{1x}Si_y system, Entropy 24 (2) (2021), https://doi.org/10.3390/ 024010002
- [79] F. Guillou, H. Yibole, B. Narsu, V. Hardy, Correlation between deformation and total entropy change at the first-order magnetic transition of Fe₂P-based magnetocaloric materials, Results Phys. 44 (2023) 106203, https://doi.org/ 10.1016/j.rinp.2022.106203.

[80] P. Roy, E. Torun, R.A. De Groot, Effect of doping and elastic properties in (Mn, Fe)₂(Si,P), Phys. Rev. B 93 (2016) 094110, https://doi.org/10.1103/PhysRevB.93.094110.

- [81] P. Roy, E. Brück, R.A. De Groot, Latent heat of the first-order magnetic transition of MnFeSi_{0.33}P_{0.66}, Phys. Rev. B 93 (2016) 165101, https://doi.org/10.1103/ PhysRevB.93.165101.
- [82] F. Guillou, H. Yibole, N.H. Van Dijk, E. Brück, Effect of boron substitution on the ferromagnetic transition of MnFe_{0.95}P_{2/3}Si_{1/3}, J. Alloys Compd. 632 (2015) 717–722, https://doi.org/10.1016/j.jallcom.2015.01.308.
- [83] M. Yue, D. Liu, Q. Huang, T. Wang, F. Hu, J. Li, G. Rao, B. Shen, J.W. Lynn, J. Zhang, Structure evolution and entropy change of temperature and magnetic field induced magneto-structural transition in Mn_{1.1}Fe_{0.9}P_{0.76}Ge_{0.24}, J. Appl. Phys. 113 (2013) 043925, https://doi.org/10.1063/1.4788803.
- [84] F. Zhang, I. Batashev, Q. Shen, Z. Wu, R.I. Smith, G.A. De Wijs, N. Van Dijk, E. Brück, Impact of F and S doping on (Mn,Fe)₂(P,Si) giant magnetocaloric materials, Acta Mater. 234 (2022) 118057, https://doi.org/10.1016/j. actamat.2022.118057.